

Reconcile the Bulk Metallic and Surface Insulating State in $1T$ -TaSe₂

Wenhao Zhang,¹ Zongxiu Wu,¹ Kunliang Bu,¹ Ying Fei,¹ Yuan Zheng,¹ Jingjing Gao,^{2,3} Xuan Luo,² Zheng Liu,⁴ Yu-Ping Sun,^{2,5,6} and Yi Yin^{1,6,*}

¹*Zhejiang Province Key Laboratory of Quantum Technology and Device, Department of Physics, Zhejiang University, Hangzhou 310027, China*

²*Key Laboratory of Materials Physics, Institute of Solid State Physics, Chinese Academy of Sciences, Hefei 230031, China*

³*University of Science and Technology of China, Hefei 230026, China*

⁴*Institute for Advanced Study, Tsinghua University, Beijing 100084, China*

⁵*High Magnetic Field Laboratory, Chinese Academy of Sciences, Hefei 230031, China*

⁶*Collaborative Innovation Center of Advanced Microstructures, Nanjing University, Nanjing 210093, China*

The transition metal dichalcogenides $1T$ -TaS₂ and $1T$ -TaSe₂ have been extensively studied for the complicated correlated electronic properties. The origin of different surface electronic states remains controversial. We apply scanning tunneling microscopy and spectroscopy to restudy the surface electronic state of bulk $1T$ -TaSe₂. Both insulating and metallic states are identified in different areas of the same sample. The insulating state is similar to that in $1T$ -TaS₂, concerning both the dI/dV spectrum and the orbital texture. With further investigations in single-step areas, the discrepancy of electronic states is found to be associated with different stacking orders. The insulating state is most possibly a single-layer property, modulated to a metallic state in some particular stacking orders. Both the metallic and large-gap insulating spectra, together with their corresponding stacking orders, are dominant in $1T$ -TaSe₂. The connected metallic areas lead to the metallic transport behavior. We then reconcile the bulk metallic and surface insulating state in $1T$ -TaSe₂. The rich phenomenon in $1T$ -TaSe₂ deepens our understanding of the correlated electronic state in bulk $1T$ -TaSe₂ and $1T$ -TaS₂.

I. INTRODUCTION

Layered transition metal dichalcogenides (TMDs) $1T$ -TaS₂ and $1T$ -TaSe₂ are two widely-studied charge density wave (CDW) materials in past few decades [1–10]. Both materials are at a commensurate CDW (CCDW) phase with a $\sqrt{13} \times \sqrt{13}$ reconstruction at low temperature. A single unpaired electron exists in each star of David (SD), the basic element of the CCDW superlattice, resulting in a half-filled system. The electron-electron correlation can split the half-filled band to the lower and upper Hubbard band (LHB and UHB) with an insulating gap, called the Mott insulator [11]. For the bulk $1T$ -TaS₂, different experimental techniques confirm the insulating gap around the Fermi level, consistent with the transport result in $1T$ -TaS₂ [5–7]. Note that the insulating gap nature of $1T$ -TaS₂ is still under debate [12–19], and is comprehensively studied in our other work [20]. For the bulk $1T$ -TaSe₂, properties measured with different techniques are more complicated [21–24]. Both scanning tunneling microscopy (STM) and angle-resolved photoemission spectroscopy (ARPES) have detected an insulating state on the exposed surface [23, 24]. However, the resistivity measurement shows a metallic behavior in the CCDW phase, also referred to as a bulk metallic state. The bulk metallic state and the surface insulating state have to be reconciled in the same material,

which is still far from a complete understanding. On the other hand, Se atoms in $1T$ -TaSe₂ share the same valence as S atoms in $1T$ -TaS₂ [25, 26]. Whether the surface insulating state in $1T$ -TaSe₂ is similar to the correlation-induced state in $1T$ -TaS₂ needs to be clarified. The insulating state in the single-layer film of $1T$ -TaSe₂/TaS₂, grown by molecular beam epitaxy (MBE), makes the problem more complicated and fascinating [27, 28].

Here we perform a detailed STM experiment to explore the electronic state of pristine $1T$ -TaSe₂ at low temperature. We find both metallic and insulating states on the exposed surface of $1T$ -TaSe₂. The insulating spectrum in $1T$ -TaSe₂ is very similar to that in $1T$ -TaS₂, from the Hubbard band features in dI/dV spectrum to the spatial orbital texture. A corrugation-induced evolution of the metallic spectrum reveals a correlation-related V-shaped feature in the metallic spectrum. With a multi-step cleaved surface, we measure and obtain three different types of dI/dV spectrum, including the large-gap spectrum, the small-gap spectrum, and the metallic spectrum, similar to those in $1T$ -TaS₂ [20]. The discrepancy of electronic states in $1T$ -TaSe₂ is found to be associated with different stacking orders. Unlike $1T$ -TaS₂ where the AA-stacking and corresponding insulating spectrum dominate, the AC-stacking and metallic state also dominate in $1T$ -TaSe₂. The bulk metallic state and surface insulating state in $1T$ -TaSe₂ are accordingly reconciled.

* yiyin@zju.edu.cn

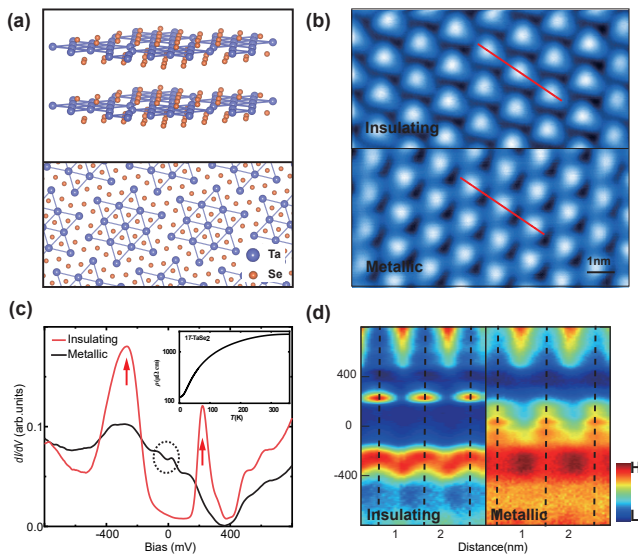


FIG. 1. Overview of structural and electronic properties of $1T$ -TaSe₂. (a) Crystal structure of $1T$ -TaSe₂. The side-view sketch is shown in the upper panel. The star-of-David (SD) is formed by 13 Ta atoms in the CCDW phase, with the top-view sketch shown in the lower panel. (b) Two 10×5 nm² topographies taken in the area of insulating (upper panel) and metallic (lower panel) state. (c) Typical dI/dV spectra taken in the area of insulating and metallic state (setup condition: $V_b = -600$ mV, $I_s = 500$ pA). The inset shows resistivity of bulk $1T$ -TaSe₂ at the range of 2–360 K, exhibiting a metallic behavior at low temperature. (d) Two linecut maps crossing three SDs along the red lines in (b). The periodic dI/dV evolution is displayed on the horizontal direction, in the bias voltage range of $[-800, 800]$ mV.

II. EXPERIMENT AND RESULTS

High-quality single crystal $1T$ -TaSe₂ was grown with the iodine transport agent. In the STM experiment, $1T$ -TaSe₂ were cleaved in situ in an ultra-high vacuum chamber (base pressure 4×10^{-11} mBar) at liquid nitrogen temperature and transferred to the STM head immediately. Topographies in this paper were collected with a bias voltage -600 mV and setpoint current 500 pA at liquid nitrogen temperature (~ 77 K). The differential conductance dI/dV spectra were acquired by the standard lock-in technique, with a voltage modulation of 10 mV at 1213.7 Hz frequency.

Bulk single crystal $1T$ -TaSe₂ has a CdI₂-type layered structure [upper panel of Fig. 1(a)]. In each unit structure, the Ta atomic layer is sandwiched between two Se atomic layers, and the Ta atoms form a triangular lattice in the plane. In the CCDW phase, every 13 Ta atoms are regrouped into a cluster called star-of-David (SD), and the SDs form an enlarged triangular super-lattice [lower panel in Fig. 1(a)]. The electronic state is strongly modified by the CCDW phase. The bands from Ta atoms are folded into three sub-bands with two filled and one half-filled [21]. In the bulk $1T$ -TaS₂, the half-filled band

is split into the LHB and UHB with a Mott insulating gap, consistent with the insulating state in the resistivity measurement. In contrast, the resistivity measurement of $1T$ -TaSe₂ [Fig. 1(c) inset] shows a metallic state at low temperature [1–3]. The discrepancy of resistivity results of $1T$ -TaS₂ and $1T$ -TaSe₂ has been explained by the different p -derived valence bands of S and Se [29–33]. However, previous ARPES and STM experiment of bulk $1T$ -TaSe₂ also observed that a surface metallic to Mott insulating phase transition occurs when the temperature is reduced to 260 K [23, 24]. The reason for the coexistence of bulk metallic and surface insulating state remains unresolved in $1T$ -TaSe₂.

A. Insulating and Metallic Electronic Spectra

In our STM experiment, the measurement temperature (≈ 77 K) is far below the CCDW transition temperature. Insulating and metallic dI/dV spectra both exist in different areas of the same sample. Figure 1(b) are two representative topographies with different electronic states. They share the same triangular SD superlattice array, with each bright spot corresponding to one SD. Figure 1(c) shows the typical insulating and metallic spectra measured at the center of one SD. The insulating dI/dV spectrum is very similar to the Mott insulating spectrum measured in bulk $1T$ -TaS₂. The LHB and UHB peaks are located at -300 and 230 mV. The gap size is around 530 mV, about 100 mV larger than that of bulk $1T$ -TaS₂ [33–35]. The CDW valley roughly at 400 mV shows an approximate zero value, suggesting a strong CDW modulation in $1T$ -TaSe₂ [26]. The metallic dI/dV spectrum displays a rough linear decay of density-of-state (DOS) around the Fermi energy (zero bias). A weak dip feature appears around the zero bias. The deep valley at 400 mV coincides with the CDW valley in the insulating dI/dV spectrum.

To show the spatial homogeneity, we present the linecut maps for both the insulating and metallic states. In Fig. 1(d), the horizontal axis is the position along the two red lines crossing three SDs in Fig. 1(b), and the vertical axis is the STM bias ranging from -800 to 800 mV. For the insulating spectra, the LHB and UHB peaks are evident at SD centers, resulting in a periodic intensity variation along the line. The CDW feature above 400 mV also shows an apparent periodic variation, but with maximum peaks shifting by half the period. This phenomenon is similar to that in $1T$ -TaS₂ [33, 34]. The Hubbard bands originate from the central Ta orbital, with LHB and UHB peaks showing maximum values at SD centers. The CDW bands are from the surrounding Ta orbital, with CDW peaks showing maximum values at midpoints between SDs. In the linecut map of metallic spectra, the zero-bias dip also shows a periodic variation, and the maximum values are located at SD centers. We expect that the two coherent peaks of the zero-bias dip in the metallic spectrum are also related to the central

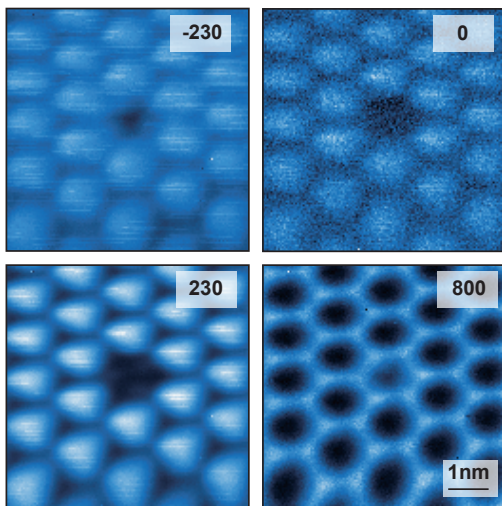


FIG. 2. The dI/dV maps at several selected energies ($-230, 0, 230, 800$ mV) for a 6×6 nm² area with insulating state. A defective SD exists in the middle of this area.

Ta orbital.

B. Orbital Texture of the Insulating State

Figure 2 displays the differential conductance dI/dV maps at several selected energies for a 6×6 nm² area with insulating state. A special point defect exists at one SD in the middle of this area, which is similar to the Ta vacancy in $1T$ -TaS₂ [20]. The dI/dV maps reveal more spatial characteristics than the linecut map crossing SDs. With the bias voltage at -230 mV and 230 mV, these two dI/dV maps are close to the LHB and UHB, respectively. Both maps show a triangular lattice pattern with the bright spots positioned at SD centers, consistent with that the Hubbard band mainly originates from the central Ta orbital. When moving to the lower energy or higher energy, the dI/dV maps reveal a honeycomb orbital texture (e.g. in the map at 800 mV), consistent with that the CDW bands are from the surrounding Ta orbitals. The energy-dependent orbital texture for the insulating state is similar to that in the bulk $1T$ -TaS₂ [33]. The single-layer MBE-grown $1T$ -TaSe₂ shows a slightly different energy-dependent orbital texture despite of the similar insulating spectrum [27, 28]. The similar insulating spectra in the single-layer and bulk samples suggest that the insulating state is most likely an intrinsic single-layer property.

C. Coherent Peaks of the Metallic State

In the metallic spectrum in Fig. 1(c), there is an asymmetric DOS distribution and a weak dip around the Fermi level. In contrast, the most metallic dI/dV spectra in $1T$ -TaS₂ display symmetric V-shaped DOS near

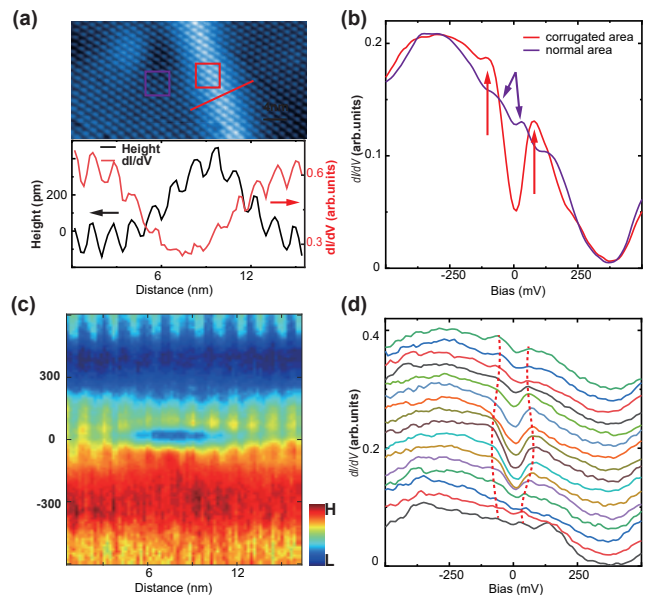


FIG. 3. The electronic state evolution in a metallic area with corrugation. (a) A 40×20 nm² topography which includes a corrugation (upper panel). Height profile and zero-bias dI/dV intensity along the red line in (a) (lower panel). (b) The averaged dI/dV spectra of the corrugated and normal areas indicated by the red and purple squares in (a). (c), (d) The linecut map and waterfall map along the red line in (a). The continuous evolution of the dI/dV spectrum across the corrugation is displayed in two ways. Extracted from a three-dimensional spectroscopy file, the linecut map has a limited resolution compared to Fig. 1(d).

the Fermi level [35–37]. The asymmetric DOS can be possibly explained by higher p -derived valence bands of Se and possible p - d hybridization in $1T$ -TaSe₂ [29, 30].

To explore more details about the metallic state, we present a modulated electronic state for the metallic phase. Previously we have found a corrugation-induced Mott-gap-collapse in $1T$ -TaS₂ [35]. The upper panel of Fig. 3(a) shows a topography with a corrugation in metallic area in $1T$ -TaSe₂, which is possibly induced by a local strain [38, 39]. The CCDW lattice is continuous throughout the area, without any domain walls. A bright stripe appears roughly in an oblique direction, with about 8 nm width. From the height profile along the red line across the corrugation [lower panel of Fig. 3(a)], the envelope of the periodic oscillation rises as a hump in the corrugation. In Fig. 3(b), we display the dI/dV spectrum averaged in the normal and corrugated areas [purple and red squares in Fig. 3(a)]. The normal area spectrum is a metallic one similar to that in Fig. 1(c), and a slight zero-bias dip shows coherent peaks at ± 30 mV. Surprisingly, the zero-bias dip in the corrugated-area spectrum is deepened, and the coherent peak positions increase to ± 80 mV.

The continuous evolution of dI/dV spectrum across the corrugation is presented in Fig. 3(c) and 3(d). The linecut map shows a periodic variation along the line, in

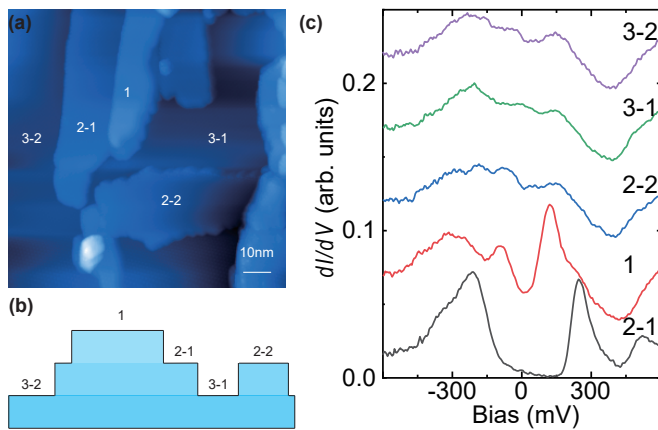


FIG. 4. Topography and corresponding electronic spectra in a multi-step area. (a) A $100 \times 100 \text{ nm}^2$ topography, with a schematic side-view shown in (b). (c) Typical dI/dV spectra on different regions in (a). The spectrum in region 3-1, 3-2 and 2-2 shows a normal metallic state of $1T\text{-TaSe}_2$, while the spectra in region 2-1 and 1 show a large-gap state and a small-gap state, respectively.

the middle of which we observe the smoothly deepened and widened zero-bias dip. The decreased zero-bias conductance is also shown in the lower panel of Fig. 3(a), together with the height profile. From the waterfall map in Fig. 3(d), the red dashed line guides the evolution of coherent peak positions, with the gap size increases to a maximum value of 80 mV in the middle of the corrugated area. From this comparison, it is reasonable to speculate that the dip is still a V-shaped gap. In the cuprate superconductor, a V-shaped spectrum represents a metallic pseudogap (PG) state evolved from the Mott insulating state [40, 41]. Different from the previous Mott-gap-collapse in corrugated area of $1T\text{-TaS}_2$ [35], here the corrugation effectively strengthens the gap size and depth. The continuous adjustment of the electronic state is possibly either from a local buckling effect or the change of interlayer distance, which is still an open question.

D. Multi-step Area and Three Types of Electronic Spectra

Although we have studied both the insulating and metallic states in-depth, the reason for the appearance of different electronic states in different regions is still a mystery. Generally speaking, $1T\text{-TaSe}_2$ has a more considerable inter-layer interaction and more charge transfer between Se and Ta compared to those in $1T\text{-TaS}_2$, which can result in different resistivity results [29, 30]. The asymmetric line shape around the Fermi energy could indicate that the Se band emerges up to the Fermi energy and mixes with the Ta band, showing a metallic DOS. This mechanism, however, cannot comprehensively explain the observed insulating state in $1T\text{-TaSe}_2$.

The insulating state in $1T\text{-TaSe}_2$ is initially explained as a Mott insulating state based on the single-layer property [25, 26]. The stacking order has been taken into account in some recent research works [12–19]. In our other work [20], a silica substrate helps to introduce single-step areas in $1T\text{-TaSe}_2$ for us to study the stacking order effect. We similarly apply a silica substrate to glue and cleave bulk $1T\text{-TaSe}_2$ [20, 43]. Figure 4(a) shows a special large area topography with multi-step environment, taken on the exposed surface of $1T\text{-TaSe}_2$. A schematic side view of this multi-step area is shown in Fig. 4(b), which is derived from the height profiles in topography. As shown in Fig. 4(c), the dI/dV spectra measured on different step planes provide very meaningful information.

For the area in Fig. 4(a), the dI/dV spectrum on the bottom layer (step 3-1 and step 3-2) is a metallic one similar to that in Fig. 1(c). On top of this layer, the dI/dV spectrum on step 2-2 is still a similar metallic one. The weak dip feature around zero bias are sometimes destroyed, and we only focus on the main background of metallic spectrum. Interestingly, the dI/dV spectra on step 2-1 is an insulating spectrum similar to that in Fig. 1(c). Furthermore, the dI/dV spectrum on step 1 has a decreased gap with coherent peaks at -70 and 140 mV. Although the zero-bias conductance of this type of spectrum is enhanced to a significant value, we call this spectrum a small-gap spectrum. The general insulating spectrum is then called a large-gap spectrum. This phenomenon reminds us the similar three types of spectra in the stacking order study in $1T\text{-TaS}_2$ [20]. Different electronic states in the same plane (step 2-1 and 2-2) imply different stacking orders between the SD super-lattices in the upper and lower layers.

E. Stacking Orders and Corresponding Spectra

To study the stacking order, we focus on the flat single-step area which renders a determination of the relative displacement of SD super-lattices in the upper and lower layers. The method is similar to that in our other work [20]. For the following shown examples, they are selected from multiple measurements on different samples. We first consider the situation with a metallic spectrum on the lower terrace. Figure 5(a)-5(c) show three single-step area topographies, which include triangular SD super-lattices in both the lower layer and the bright upper layer. The spectra measured on the lower and upper terraces are shown in Fig. 5(d)-5(f). On the upper terrace, the electronic state shows a metallic spectrum, a large-gap spectrum, and a small-gap spectrum for the three cases, respectively. After determining the relative shift between the two SD super-lattices, we find that the three cases correspond to the AC-stacking, the AA-stacking, and the AB-stacking, respectively [Fig. 5(g)-5(i)].

For the AA-stacking case, the dI/dV spectrum measured on the upper terrace is a large-gap spectrum when

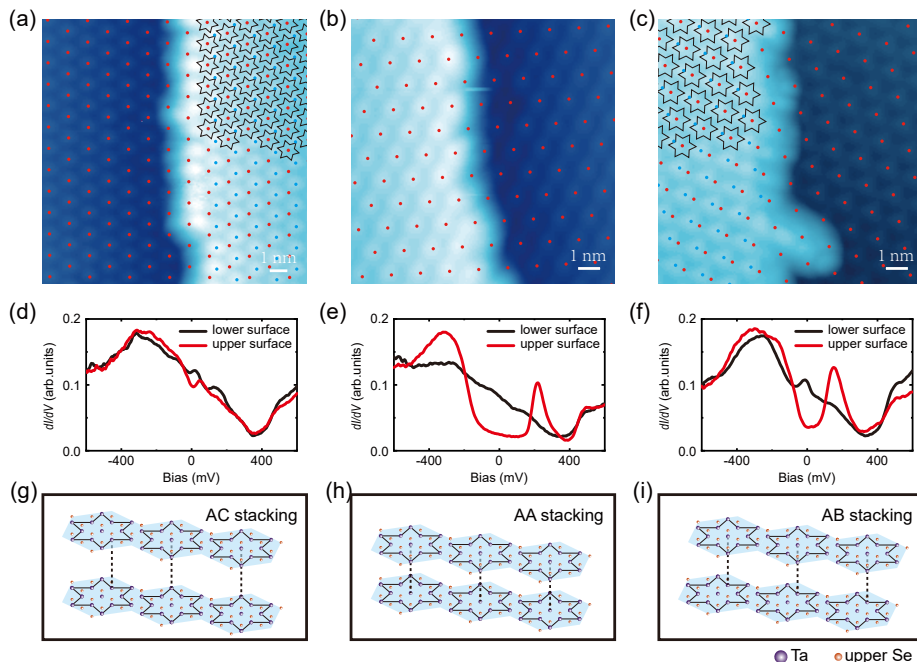


FIG. 5. The stacking orders and corresponding dI/dV spectra with a bottom metallic spectrum. (a) STM topography of a single-step area. The red (blue) dots mark SD centers in the lower (upper) layer. The SD centers in the upper layer are aligned with the SD outer-corner sites in the lower layer, or in the AC-stacking order. (b), (c) STM topographies of two other single-step areas, in the AA-stacking or AB-stacking orders as shown in the superimposed SD centers. (d)-(f) The red and black lines are the dI/dV spectra on the upper and lower terraces in (a)-(c). (h)-(i) The schematic diagrams of the stacking orders in (a)-(c).

the SD center in one layer is vertically aligned with the SD center in the underlying layer, which is consistent with the stacking rule in $1T$ -TaS₂ [20]. In the AC-stacking case, when the SD center in one layer is vertically aligned with the outer-corner site of SD in the underlying layer, the dI/dV spectrum measured on the upper terrace is a metallic spectrum, which is different from the small-gap spectrum in $1T$ -TaS₂ [20]. The discrepancy also happens in the AB-stacking case, when the SD center in one layer is vertically aligned with the inner-corner site of SD in the underlying layer, which corresponds to a small-gap spectrum in $1T$ -TaSe₂ but a metallic spectrum in $1T$ -TaS₂. With multiple measurements, we find that the AC-stacking and AA-stacking cases are more frequent, and the corresponding spectra are constantly reproducible. Both the AB-stacking with a metallic spectrum in $1T$ -TaS₂ and the AB-stacking with a small-gap spectrum in $1T$ -TaSe₂ only occasionally appear.

We further consider the situation with an insulating spectrum on the lower terrace, which is also commonly seen in $1T$ -TaSe₂. Different from $1T$ -TaS₂, the AA-stacking only occasionally appear in this situation in $1T$ -TaSe₂, although the large-gap spectrum has been observed on the upper terrace (not shown). Figure 6(a)-6(c) show three single-step area topographies, with the spectra measured on the lower and upper terraces shown in Fig. 6(d)-6(f). On the upper terrace, the electronic state shows an insulating spectrum, a metallic spectrum,

and another metallic spectrum for the three cases, respectively. After determining the stacking order, we find that Fig. 6(a)-6(b) correspond to the AC-stacking and the AC'-stacking, respectively. In the AC-stacking and AC'-stacking, the SD center in one layer is vertically aligned with two types of unequivalent outer-corner of SDs in the underlying layer. Figure 6(c) corresponds to the AB-stacking order. With multiple measurements, we find that these three cases are all frequent and constantly reproducible. Then we can see that the upper terrace spectrum is not only related to the stacking order, but also to the spectrum in the lower terrace. The AC-stacking corresponds to a metallic spectrum in Fig. 5(a) but an insulating spectrum in Fig. 6(a).

Figure 7 shows two uncommon examples, for the situation with an insulating spectrum on the lower terrace. The upper-terrace spectrum in both cases is a small-gap spectrum [Fig. 7(b)-7(e)], under an AC-stacking and an AB-stacking orders, respectively. In Fig. 7 and Fig. 6, the same stacking order and lower-terrace spectrum can lead to different results suggests that other factors may have played a role. We do not exclude that other uncommon cases could occur. The small-gap spectrum is prone to be classified as an intermediate spectrum between the insulating large-gap spectrum and the metallic spectrum. The delicate spectrum variation of each type originates from different tips or the condition details.

In Fig. 6(a), the AC-stacking order corresponds to

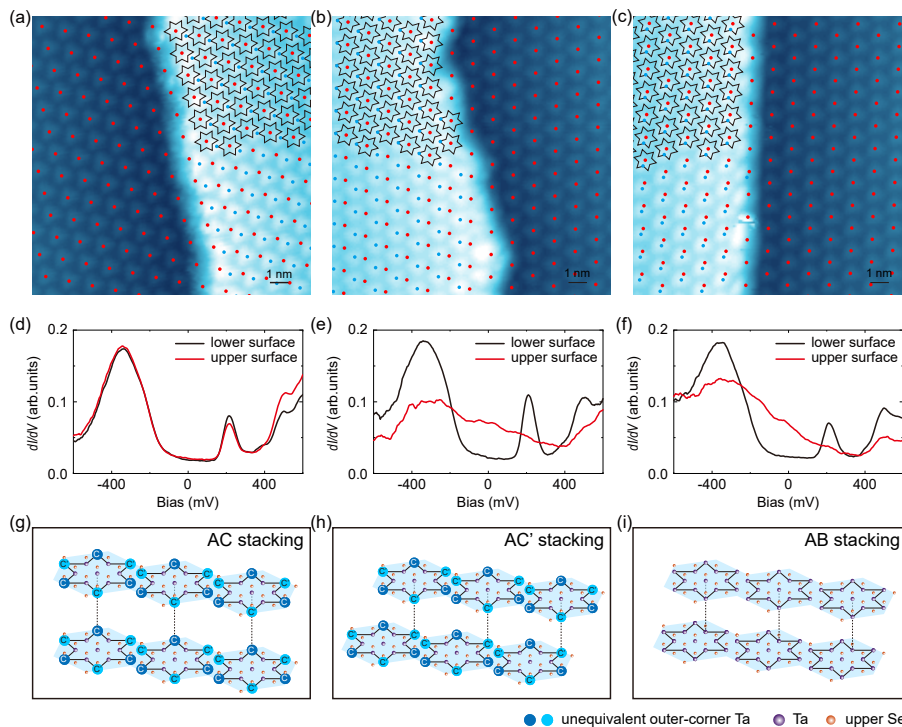


FIG. 6. The stacking orders and corresponding dI/dV spectra with a bottom insulating spectrum. (a) STM topography of a single-step area. The red (blue) dots mark SD centers in the lower (upper) layer. The SD centers in the upper layer are aligned with the SD outer-corner sites in the lower layer, or in the AC-stacking order. (b), (c) STM topographies of two other single-step areas, in the AC'-stacking or AB-stacking orders as shown in the superimposed SD centers. (d)-(f) The red and black lines are the dI/dV spectra on the upper and lower terraces in (a)-(c). (h)-(i) The schematic diagrams of the stacking orders in (a)-(c).

two large-gap spectra on both the upper and lower terraces, which deny that the large gap is from the unit-cell doubling of two AA-stacked layers [16–18]. The large-gap spectrum is most possibly the intrinsic property of a single-layer $1T$ -TaSe₂, similar to that of MBE grown film of $1T$ -TaSe₂. The metallic spectrum is not intrinsic in the single-layer $1T$ -TaSe₂, but a modulated spectrum induced by particular stacking orders. From the most common cases we can summarize the stacking order phenomenon in $1T$ -TaSe₂. On top of the insulating layer, a metallic layer can be induced by the AC'-stacking and AB-stacking orders. The AC-stacking can further allow a new metallic layer to be stacked on top of the metallic layer. On top of the metallic layer, an insulating layer can be induced by the AA-stacking order. The AC-stacking can further allow a new insulating layer to be stacked on top of the insulating layer. In $1T$ -TaSe₂, both the metallic state and large-gap insulating state can extend all the way at the step edge, although only the large-gap spectrum can extend all the way in $1T$ -TaS₂. The difference is consistent with that insulating state and metallic state can appear at different regions in the same sample in $1T$ -TaSe₂, while only the insulating state dominates in $1T$ -TaS₂. Please note that although we can only measure the spectrum on exposed terraced areas, the collected information helps to predict the electronic state layer-by-

layer when we know the state of underlying layer and the stacking order.

III. CONCLUSION

Combining all the above information, we demonstrate that the stacking order plays a crucial role in determining the surface electronic state in pristine $1T$ -TaSe₂. The main difference between $1T$ -TaS₂ and $1T$ -TaSe₂ is that, the AA-stacking and corresponding large-gap insulating spectrum dominate in $1T$ -TaS₂, while many different stacking orders are able to induce both insulating and metallic states depending on the electronic states of the underlying layer in $1T$ -TaSe₂. A large enough ratio of metallic state can always yield a metallic state in the macroscopic transport measurement.

The in-plane electron-electron correlation exists in both the insulating and metallic states. In pristine $1T$ -TaSe₂, the large-gap insulating state mainly reflects the intrinsic single-layer Mott gap, while some spectral details like the nonzero conductance around the Fermi energy and the slope from LHB to zero bias position may be related to the inter-layer effect along the c -axis. In general, the inter-layer coupling plays a stronger role in $1T$ -TaSe₂ than in $1T$ -TaS₂. The extremely easy mod-

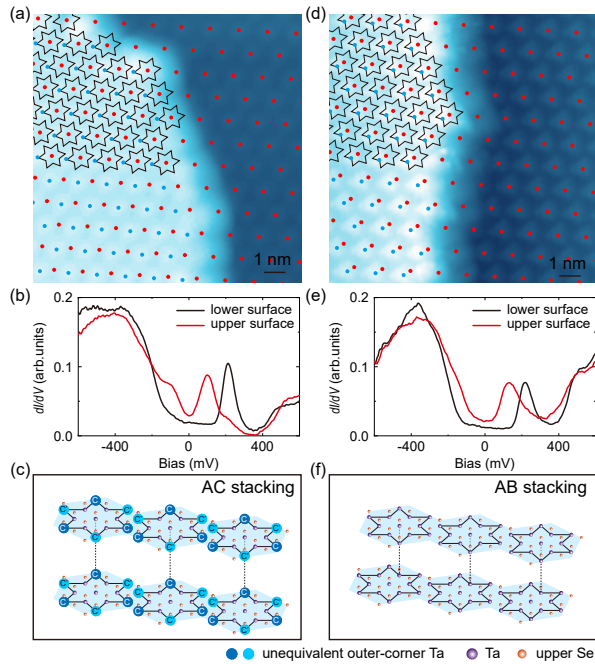


FIG. 7. The stacking orders of small-gap states with a bottom insulating spectrum. (a) STM topography of a single-step area. The red (blue) dots mark SD centers in the lower (upper) layer. The SD center in the upper layer is aligned with the SD outer-corner site in the lower layer, or in the AC-stacking order. (b) The red and black lines are the dI/dV spectra on the upper and lower terraces in (a). (c) The schematic diagram of the AC-stacking order. (d)-(f) STM topography, corresponding dI/dV spectra on the upper and lower terraces, and the schematic diagram of the AB-stacking order in another single-step area.

ulation of the electronic state can also make the MBE film slightly different from the insulating state in bulk sample, possibly related to the substrate-induced effect or the particular growth condition. The Mott physics in TMD materials $1T$ -TaSe₂ and $1T$ -TaS₂ is proved to be exceptionally rich and deserves further exploration.

ACKNOWLEDGMENTS

This work was supported by the National Key Research and Development Program of China (Grants No. 2019YFA0308602), the Key Research and Development Program of Zhejiang Province, China (2021C01002), and the Fundamental Research Funds for the Central Universities in China. Z.L. thanks the National Nature Science Foundation of China (NSFC-11774196) and Tsinghua University Initiative Scientific Research Program. J.J.G., X.L., and Y.P.S. thank the support of the National Key Research and Development Program of China (Grants No. 2016YFA0300404), the National Nature Science Foundation of China (NSFC-11674326 and NSFC-11874357), the Joint Funds of the National Natural Science Foundation of China, and the Chinese Academy of Sciences' Large-Scale Scientific Facility (U1832141, U1932217, U2032215).

- [1] J. A. Wilson, F. J. Di Salvo, and S. Mahajan, Charge-Density Waves and Superlattices in the Metallic Layered Transition Metal Dichalcogenides, *Adv. Phys.* **24**, 117 (1975).
- [2] F. J. Di Salvo, J. A. Wilson, B. G. Bagley, and J. V. Waszczak, Effects of Doping on Charge-Density Waves in Layer Compounds, *Phys. Rev. B* **12**, 2220 (1975).
- [3] P. Fazekas and E. Tosatti, Electrical, Structural and Magnetic Properties of Pure and Doped $1T$ -TaS₂, *Philos. Mag. B* **39**, 229 (1979).
- [4] K. Rossnagel, On the Origin of Charge-Density Waves in Select Layered Transition-Metal Dichalcogenides, *J. Phys.: Condens. Matter* **23**, 213001 (2011).
- [5] J. J. Kim, W. Yamaguchi, T. Hasegawa, and K. Kitazawa, Observation of Mott Localization Gap Using Low Temperature Scanning Tunneling Spectroscopy in Commensurate $1T$ -TaS₂, *Phys. Rev. Lett.* **73**, 2103 (1994).
- [6] J. J. Kim, I. Ekvall, and H. Olin, Temperature-Dependent Scanning Tunneling Spectroscopy of $1T$ -TaS₂, *Phys. Rev. B* **54**, 2244 (1996).
- [7] N. V. Smith, S. D. Kevan, and F. J. DiSalvo, Band Structures of the Layer Compounds $1T$ -TaS₂ and $1H$ -TaSe₂ in the Presence of Commensurate Charge-Density Waves, *J. Phys. C: Solid State Phys.* **18**, 3175 (1985).
- [8] B. Sipos, A. F. Kusmartseva, A. Akrap, H. Berger, L. Forró, and E. Tutiš, From Mott State to Superconductivity in $1T$ -TaS₂, *Nat. Mater.* **7**, 960 (2008).
- [9] I. Lutsyk, M. Rogala, P. Dabrowski, P. Krukowski, P. J. Kowalczyk, A. Busiakiewicz, D. A. Kowalczyk, E. Laciniska, J. Binder, N. Olszowska, M. Kopciuszynski, K. Szalowski, M. Gmitra, R. Stepniewski, M. Jalochowski, J. J. Kolodziej, A. Wyszomolek, and Z. Klusek, Electronic Structure of Commensurate, Nearly Commensurate, and Incommensurate Phases of $1T$ -TaS₂ by Angle-Resolved Photoelectron Spectroscopy, Scanning Tunneling Spectroscopy, and Density Functional Theory, *Phys. Rev. B* **98**, 195425 (2018).
- [10] E. Lahoud, O. N. Meetei, K. B. Chaska, A. Kanigel, and N. Trivedi, Emergence of a Novel Pseudogap Metallic State in a Disordered 2D Mott Insulator, *Phys. Rev. Lett.* **112**, 206402 (2014).
- [11] N. F. Mott, Metal-Insulator Transition, *Rev. Mod. Phys.* **40**, 677 (1968).
- [12] T. Ritschel, J. Trinckauf, K. Koepf, B. Büchner, M. v. Zimmermann, H. Berger, Y. I. Joe, P. Abbamonte, and J. Geck, Orbital Textures and Charge Density Waves in Transition Metal Dichalcogenides, *Nat. Phys.* **11**, 328 (2015).

- (2015).
- [13] T. Ritschel, H. Berger, and J. Geck, Stacking-Driven Gap Formation in Layered $1T$ -TaS₂, *Phys. Rev. B*, **98**, 195134 (2018).
- [14] S. H. Lee, J. S. Goh, and D. Cho, Origin of the Insulating Phase and First-Order Metal-Insulator Transition in $1T$ -TaS₂, *Phys. Rev. Lett.* **122**, 106404 (2019).
- [15] D. B. Shin, T. -D. Nicolas, J. Zhang, M. S. Okyay, A. Rubio, and N. Park, Identification of the Mott Insulating Charge Density Wave State in $1T$ -TaS₂, *Phys. Rev. Lett.* **126**, 196406 (2021).
- [16] C. J. Butler, M. Yoshida, T. Hanaguri, and Y. Iwasa, Mottness versus Unit-Cell Doubling as the Driver of the Insulating State in $1T$ -TaS₂, *Nat. Commun.* **11**, 2477 (2020).
- [17] C. J. Butler, M. Yoshida, T. Hanaguri, and Y. Iwasa, Doublonlike Excitations and Their Phononic Coupling in a Mott Charge-Density-Wave System, *Phys. Rev. X* **11**, 011059 (2021).
- [18] J. Lee, K.-H. Jin, H. W. Yeom, Distinguishing a Mott Insulator from a Trivial Insulator with Atomic Adsorbates, *Phys. Rev. Lett.* **126**, 196405 (2021).
- [19] Y. D. Wang, W. L. Yao, Z. M. Xin, T. T. Han, Z. G. Wang, L. Chen, C. Cai, Y. Li, and Y. Zhang, Band Insulator to Mott Insulator Transition in $1T$ -TaS₂, *Nat. Commun.* **11**, 4215 (2020).
- [20] Z. Wu, K. Bu, W. Zhang, Y. Fei, Y. Zheng, J. Gao, X. Luo, Z. Liu, Y.-P. Sun, and Y. Yin, Effect of Stacking Order on the Electronic State of $1T$ -TaS₂ arXiv:2105.08663
- [21] K. Horiba, K. Ono, J. H. Oh, T. Kihara, S. Nakazono, M. Oshima, O. Shiino, H. W. Yeom, A. Kakizaki, and Y. Aiura, Charge-Density Wave and Three-Dimensional Fermi Surface in $1T$ -TaSe₂ Studied by Photoemission Spectroscopy, *Phys. Rev. B* **66**, 073106 (2002)
- [22] J. J. Kim, W. Yamaguchi, T. Hasegawa, and K. Kitazawa, Site-Specified Tunneling Spectroscopy of Local Sensity of States in the Charge-Density-Wave State of $1T$ -TaSe₂ at 77 K, *Phys. Rev. B* **50**, 4958(R) (1994).
- [23] L. Perfetti, A. Georges, S. Florens, S. Biermann, S. Mitrovic, H. Berger, Y. Tomm, H. Höchst, and M. Grioni, Spectroscopic Signatures of a Bandwidth-Controlled Mott Transition at the Surface of $1T$ -TaSe₂, *Phys. Rev. Lett.* **90**, 166401 (2003).
- [24] S. Colonna, F. Ronci, A. Cricenti, L. Perfetti, H. Berger, and M. Grioni, Mott Phase at the Surface of $1T$ -TaSe₂ Observed by Scanning Tunneling Microscopy, *Phys. Rev. Lett.* **94**, 036405 (2005).
- [25] P. Darancet, A. J. Millis, and C. A. Marianetti, Three-Dimensional Metallic and Two-Dimensional Insulating Behavior in Octahedral Tantalum Dichalcogenides, *Phys. Rev. B* **90**, 045134 (2014).
- [26] Y. Z. Ge and A. Y. Liu, First-Principles Investigation of the Charge-Density-Wave Instability in $1T$ -TaSe₂, *Phys. Rev. B* **82**, 155133 (2010).
- [27] Y. Chen, W. Ruan, M. Wu, S. Tang, H. Ryu, H. Z. Tsai, R. Lee, S. Kahn, F. Liou, C. Jia, Oliver R. Albertini, H. Xiong, Tao Jia, Z. Liu, J. A. Sobota, A. Y. Liu, J. E. Moore, Z. X. Shen, S. G. Louie, S. K. Mo, and M. F. Crommie, Strong Correlations and Orbital Texture in Single-Layer $1T$ -TaSe₂, *Nat. Phys.* **16**, 218 (2020).
- [28] H. Lin, W. Huang, K. Zhao, S. Qiao, Z. Liu, J. Wu, X. Chen, and S. H. Ji, Scanning Tunneling Spectroscopic Study of Monolayer $1T$ -TaS₂ and $1T$ -TaSe₂, *Nano Res.* **13**, 133 (2020).
- [29] F. Clerc, M. Bovet, H. Berger, L. Despont, C. Koitzsch, O. Gallus, L. Patthey, M. Shi, J. Krempasky, M. G. Garnier, and P. Aebi, Spin-Orbit Splitting in the Valence Bands of $1T$ -TaS₂ and $1T$ -TaSe₂, *J. Phys. Condens. Matter* **16**, 3271 (2004).
- [30] M. Bovet, D. Popović, F. Clerc, C. Koitzsch, U. Probst, E. Bucher, H. Berger, D. Naumović, and P. Aebi, Pseudogapped Fermi Surfaces of $1T$ -TaS₂ and $1T$ -TaSe₂: A Charge Density Wave Effect, *Phys. Rev. B* **69**, 125117 (2004).
- [31] Y. Liu, R. Ang, W. J. Lu, W. H. Song, L. J. Li, and Y. P. Sun, Superconductivity Induced by Se-Doping in Layered Charge-Density-Wave System $1T$ -TaS_{2-x}Se_x, *Appl. Phys. Lett.* **102**, 192602 (2013)
- [32] R. Ang, Y. Miyata, E. Ieki, K. Nakayama, T. Sato, Y. Liu, W. J. Lu, Y. P. Sun, and T. Takahashi, Superconductivity and Bandwidth-Controlled Mott Metal-Insulator Transition in $1T$ -TaS_{2-x}Se_x, *Phys. Rev. B* **90**, 166401 (2003)
- [33] S. Qiao, X. T. Li, N. Z. Wang, W. Ruan, C. Ye, P. Cai, Z. Q. Hao, H. Yao, X. H. Chen, J. Wu, Y. Y. Wang, and Z. Liu, Mottness Collapse in $1T$ -TaS_{2-x}Se_x Transition-Metal Dichalcogenide: An Interplay between Localized and Itinerant Orbitals, *Phys. Rev. X* **7**, 041054 (2017).
- [34] D. Cho, Y. H. Cho, S. W. Cheong, K. S. Kim, and H. W. Yeom, Interplay of Electron-Electron and Electron-Phonon Interactions in the Low-Temperature Phase of $1T$ -TaS₂, *Phys. Rev. B* **92**, 085132 (2015).
- [35] K. L. Bu, W. H. Zhang, Y. Fei, Z. X. Wu, Y. Zheng, J. J. Gao, X. Luo, Y. P. Sun, and Y. Yin, Possible Strain Induced Mott Gap Collapse in $1T$ -TaS₂, *Commun. Phys.* **2**, 146 (2019).
- [36] L. Ma, C. Ye, Y. Yu, X. F. Lu, X. Niu, S. Kim, D. Feng, D. Tománek, Y. W. Son, X. H. Chen, and Y. B. Zhang, A Metallic Mosaic Phase and the Origin of Mott-Insulating State in $1T$ -TaS₂, *Nat. Commun.* **7**, 10956 (2016).
- [37] D. Cho, S. Cheon, K. S. Kim, S. H. Lee, Y. H. Cho, S. W. Cheong, and H. W. Yeom, Nanoscale Manipulation of the Mott Insulating State Coupled to Charge Order in $1T$ -TaS₂, *Nat. Commun.* **7**, 10453 (2016).
- [38] D. Edelberg, H. Kumar, V. Shenoy, H. Ochoa, and A. N. Pasupathy, Tunable Strain Soliton Networks Confine Electrons in Van der Waals Materials, *Nat. Phys.* **16**, 1097 (2020).
- [39] L. Meng, W. Y. He, H. Zheng, M. Liu, H. Yan, W. Yan, Z. D. Chu, K. Bai, R. F. Dou, Y. Zhang, Z. Liu, J. C. Nie, and L. He Strain-Induced One-Dimensional Landau Level Quantization in Corrugated Graphene, *Phys. Rev. B* **87**, 205405 (2013).
- [40] P. Cai, W. Ruan, Y. Y. Peng, C. Ye, X. T. Li, Z. Q. Hao, X. J. Zhou, D. H. Lee, and Y. Y. Wang, Visualizing the Evolution from the Mott Insulator to a Charge-Ordered Insulator in Lightly Doped Cuprates, *Nat. Phys.* **12**, 1047 (2016).
- [41] B. Keimer, S. A. Kivelson, M. R. Norman, S. Uchida, and J. Zaanen, From Quantum Matter to High-Temperature Superconductivity in Copper Oxides, *Nature* **518**, 179 (2015).
- [42] J. Skolimowski, Y. Gerasimenko, and R. Žitko, Mottness Collapse without Metallization in the Domain Wall of the Triangular-Lattice Mott Insulator $1T$ -TaS₂, *Phys. Rev. Lett.* **122**, 036802 (2019).
- [43] S. Gao, F. Flicker, R. Sankar, H. Zhao, Z. Ren, B. Rachmilowitz, S. Balachandar, F. Chou, K. S. Burch,

Z. Wang, J. van Wezel, and I. Zeljkovic, Atomic-Scale

Strain Manipulation of a Charge Density Wave, Proc. Natl. Acad. Sci. USA **115**, 6986 (2018).